OPEN ACCESS

Applied Physics Express **11**, 065102 (2018)

https://doi.org/**10.7567/APEX.11.065102**

Ultra-high-speed graphene optical modulator design based on tight field confinement in a slot waveguide

Goran Kovacevic[1]*, Christopher Phare[2], Sze Y. Set[1], Michal Lipson[2], and Shinji Yamashita[1]*

[1]*Research Center for Advanced Science and Technology (RCAST), University of Tokyo, Meguro, Tokyo 153-8904, Japan*
[2]*School of Engineering and Applied Science, Columbia University, New York, NY 10027, U.S.A.*

*E-mail: gorank@cntp.t.u-tokyo.ac.jp; syama@cntp.t.u-tokyo.ac.jp

Received April 5, 2018; accepted April 27, 2018; published online May 23, 2018

We present a design of an ultra-fast in-line graphene optical modulator on a silicon waveguide with a bandwidth exceeding 100 GHz, very small power consumption below 15 fJ/bit, and insertion loss of 1.5 dB. This is achieved by utilizing the transverse-electric-mode silicon slot to tailor the overlap of graphene electrodes, thus significantly reducing the capacitance of the device while maintaining a low insertion loss and using conservative estimates of the graphene resistance. Our design is substantiated by comprehensive finite-element-method simulations and RC circuit characterization, as well as fabrication feasibility discussion. © 2018 The Japan Society of Applied Physics

Since the first successful fabrication of monolayer graphene in 2004,[1)] there has been a significant interest for its application in various fields of applied physics.[2,3)] In the optical domain, graphene exhibits a large light–matter interaction exemplified by the strong absorption, which is largely wavelength-independent.[4)] This paved the way for use of graphene as a light–matter-interaction-enhancing material in optics, particularly in silicon photonics,[5)] where silicon exhibits an intrinsically low light–matter ineraction.[6)] Recently, many graphene-enhanced integrated photonic devices have been proposed, such as photodetectors,[7,8)] polarizers,[9,10)] various plasmonic devices,[11,12)] and modulators,[13,14)] which are the focus of this study.

Graphene-based modulators have significantly advanced since their introduction in 2011;[13)] however, their performance remains limited by the relatively low response bandwidth and large power consumption. This is a fundamental issue arising from the monolayer structure of graphene, which limits the interaction with optical fields and requires large sheets of graphene to obtain a useful device performance. Large graphene sheets ultimately increase the RC constant of devices, limiting the speed and power consumption. The highest reported bandwidth is 30 GHz on a ring resonator structure;[15)] however, in order to properly utilize graphene in silicon photonic devices the bandwidth should cross the 100 GHz mark.[16)] There has been no experimental report of a 100 GHz graphene modulator; such modulator designs have been mentioned in the literature by Meng et al.,[10)] where less conservative values for the graphene resistance were assumed, and Wu et al.,[17)] based on a ring resonator (i.e., not in-line) posing a significant fabrication challenge with a small resistance. It has been suggested that the only approach to reduce the RC constant in graphene devices is to perform further technological advancements in graphene fabrication, which would reduce the resistance of graphene.[5,13)] In this study, we propose an in-line graphene modulator, whose bandwidth crosses the 100 GHz mark, while assuming conservative values for the graphene resistance, which were experimentally obtained in previous studies. This is achieved by proposing a partial overlap of graphene electrodes over the waveguide region, which significantly reduces the capacitance of the device, and utilizing the silicon slot waveguide to limit the insertion loss (IL), as it was recently demonstrated to enhance the graphene absorption when covered with graphene.[18,19)] We substantiate our design with finite-element simulations and equivalent RC circuit characterization, and focus on the fabrication challenges.

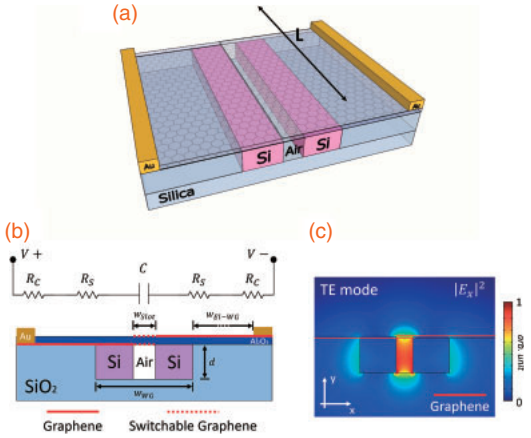

Fig. 1. (a) Three-dimensional schematic of the modulator design with the device length parameter L (not in scale). (b) Cross-section of the device with the equivalent RC circuit. The parameters are: $w_{WG} = 540$ nm and $d = 210$ nm for different slot widths w_{Slot}, and $w_{El-WG} = 1$ μm (not shown in scale). (c) Mode profile of the device.

The scheme and principle of operation of the proposed modulator are presented in Fig. 1. The device consists of a silicon slot waveguide, covered with two graphene layers partially overlapped only over the slot region of the waveguide and separated by a thin aluminum-oxide dielectric, which forms a graphene capacitor. The main principle of operation of the modulator is the same as that proposed by Liu et al.,[14)] where when a voltage is applied to the graphene electrodes, a simultaneous electron doping in one electrode and electron depletion in the other electrode occur, causing a Fermi-energy shift and changes in absorption and refractive index in the capacitor region.

The uniqueness of our design is the partial graphene electrode overlap over the waveguide (in contrast to the full waveguide overlap in all of the previous reports). It reduces the effective width of the capacitor and capacitance by more

than one order of magnitude, enabling bandwidths larger than 100 GHz and energy consumption smaller than 15 fJ/bit, as the accumulation and depletion of electrons occur only in the overlapped part of the graphene electrodes, making the width of the graphene capacitor effectively only equal to the slot width in our design. A negative effect is that if the graphene electrodes are partially overlapped on top of the waveguide, the non-overlapped graphene will not experience electrical doping and shift of the Fermi level, thus it will absorb and cause IL. This principle of operation is graphically explained in Fig. 1(b), where we differentiate between "switchable" and "non-switchable" graphene. In our previous study, where we assumed regular silicon waveguides, this IL was too large to obtain any significant improvement in performance compared to existing devices.[20] By utilizing the silicon slot waveguides, the overlap of the graphene electrodes can be significantly reduced, while still maintaining a low IL, owing to the tight field confinement inside the slot, where graphene is "switchable" [Fig. 1(c)].

Our design, which utilizes transverse-electric-(TE)-mode silicon slot waveguides, makes the modulator polarization dependent; however, with the emergence of efficient integrated polarization rotators, this is not a general drawback.[21,22]

We calculate the passive parameters of our device: modulation depth (MD), IL, and maximum refractive index change (Δn); the obtained values are MD = 0.195 dB/μm, IL = 0.09 dB/μm, and $\Delta n \approx 0.008$, for an average target slot width of 50 nm (Fig. 2). The MD is associated with the electro-absorption regime of the modulator, while Δn describes the phase-modulation regime. In order to calculate these parameters, we employed the two-dimensional (2D) finite element method through the COMSOL Multiphysics software and obtained the complex effective refractive index of our device, n_{eff}. The MD and IL parameters were calculated from the absorption parameter $\alpha = 2\,\mathrm{Im}(n_{\mathrm{eff}})k_0$, assuming $P_{\mathrm{out}} = P_{\mathrm{in}}\exp(-\alpha z)$, while Δn was calculated from the real part of n_{eff}. We consider graphene through its surface dynamic conductivity and magnetic field boundary condition $\boldsymbol{n}x(\boldsymbol{H}_1 - \boldsymbol{H}_2) = \boldsymbol{J}_s = \sigma \boldsymbol{E}_{\parallel}$,[23] which is implemented in COMSOL through surface currents. The surface currents are proportional to the surface conductivity σ multiplied by the in-graphene-plane electric fields, thus ensuring that graphene interacts only with the in-plane fields. Graphene outside the electrode overlapping region is assumed to have the graphene's intrinsic dynamic conductivity:[4] $\sigma_0 = e^2/4\hbar \approx 60\,\mu\mathrm{S}$, while the "switchable" graphene in the graphene capacitor is expressed by[24]

$$\sigma = \frac{\sigma_0}{2}\left[\tanh\left(\frac{\hbar\omega + 2E_{\mathrm{F}}}{4k_{\mathrm{B}}T}\right) + \tanh\left(\frac{\hbar\omega - 2E_{\mathrm{F}}}{4k_{\mathrm{B}}T}\right)\right] - i\frac{\sigma_0}{2\pi}\log\left[\frac{(\hbar\omega + 2E_{\mathrm{F}})^2}{(\hbar\omega - 2E_{\mathrm{F}})^2 + (2k_{\mathrm{B}}T)^2}\right] + i\frac{4\sigma_0}{\pi}\frac{E_{\mathrm{F}}}{\hbar\omega + i\hbar\gamma}. \quad (1)$$

The first two terms correspond to the real and imaginary contributions of inter-band transitions, while the final term corresponds to intra-band transitions. In all of the simulations, we assume a light wavelength of 1,550 nm and room temperature of 300 K. The γ term in Eq. (1) corresponds to the inverse scattering time in graphene, which varies from 10 fs to larger than 1,000 fs in the literature; we use an average time of 100 fs in our simulations.[24,25] The Fermi energy of graphene is related to the applied voltage through

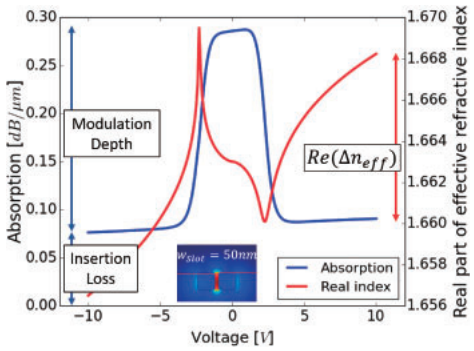

Fig. 2. Dependences of the absorption and real part of the effective index on the applied voltage for the proposed modulator for a fixed slot width of 50 nm.

the formula: $E_{\mathrm{F}} = \mathrm{sgn}(V)\hbar v_{\mathrm{F}}\sqrt{\pi\varepsilon_0\varepsilon_{\mathrm{Al_2O_3}}|V|/d_{\mathrm{Al_2O_3}}e}$, where we use a Fermi velocity, v_{F}, of 10^6 m/s, and assume $\varepsilon_{\mathrm{Al_2O_3}} = 9.72$ and $d_{\mathrm{Al_2O_3}} = 10$ nm, similar to those in the previous reports. With these assumptions, we plot the parameters' dependence on the voltage, as shown in Fig. 2. The geometric characteristics of our device: Full width of the waveguide of $w_{\mathrm{WG}} = 540$ nm and height of $d = 210$ nm [Fig. 1(b)], satisfy the single-mode operation. We also assume an air slot, which amplifies the slot effect, and is the most feasible assumption with respect to fabrication limitations, as explained at the end of this paper. Figure 2 further exemplifies the uniqueness of our design; even in the "On" regime (high voltage), there is a significant absorption corresponding to the "non-switchable" part of graphene; however, it is more than twice lower than the MD owing to the slot effect.

In Fig. 3, we characterize the IL properties of our device in detail, owing to the low-IL condition of silicon photonics.[16] In Fig. 3(a), we focus on the electro-absorption regime and plot the IL and MD, as defined in Fig. 2, as well as total loss (TL, equal to MD + IL in log scale), with respect to the slot width. The TL and IL were calculated assuming applied voltages of 0 and 10 V, respectively. The 50 nm slot width (overlap of the graphene electrodes) is indeed the optimal choice, as the total absorption has a maximum at this point, with MD more than twice larger than the IL (MD = 0.195 dB/μm, IL = 0.09 dB/μm, TL = 0.285 dB/μm). This implies that if we choose the length of our device such that a 3 dB modulation depth is achieved, the IL would be smaller than 1.5 dB, which is a small penalty to achieve very large bandwidths and small energy consumption. The result in Fig. 3(a) shows that for any slot width in the range of 15 to 140 nm, the MD is at least as large as the IL, demonstrating the usability of even larger slot widths (graphene overlaps), which might pose a smaller fabrication challenge. The absorption peak around 50 nm for a graphene-covered slot device is also in agreement with previous studies on graphene slot modulators and graphene-on–slot-waveguide effect,[18,19] and is on the order of magnitude of graphene absorption in optimized waveguide geometries.[26]

Further, we consider the potential for this structure to be used as a phase modulator. Recently, graphene-based phase modulators have attracted a significant attention,[25,27,28] as for high voltages, the TL of graphene is low and constant, while there is a significant change in the real refractive index (Fig. 2). However, the proposed and demonstrated modulators

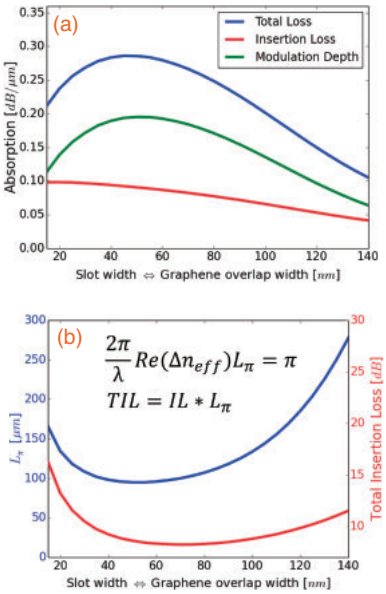

Fig. 3. (a) Properties of the modulator in the electro-absorption regime: total absorption, IL, and MD with respect to different slot widths. (b) Properties of the modulator in the phase modulation regime: π-phase-change length and corresponding IL with respect to different slot widths.

also suffer from large response times, well below the 40 GHz mark. In Fig. 3(b), we simulate the phase modulation characteristics of our device, with a focus on the IL; L_π is the length of the device required to achieve a phase shift of π, where $\mathrm{Re}(\Delta n_{\mathrm{eff}})$ is calculated as in Fig. 2, while the total IL is calculated by multiplying the L_π length and IL shown in Fig. 3(a). Even though our device exhibits a very small L_π, comparable to those reported previously,[19] the IL is always larger than 8 dB. Therefore, even though our structure would provide a significant benefit in terms of response bandwidth and energy consumption, the IL is too large to be used as a phase modulator and can be used only in the electro-absorption regime.

We confirm the ultra-high-speed performance of our device by calculating the response bandwidth, which yields a value of $B = 120$ GHz for a 50 nm slot width (graphene overlap); the bandwidths reach 400 GHz for smaller slot widths, and are always larger than 50 GHz for larger slot widths (Fig. 4), assuming conservative values for the graphene resistance. In order to calculate the bandwidth, we define an equivalent RC circuit of our device, shown in Fig. 1(b); R_C and R_S are the contact and sheet resistances of graphene, respectively, and C is the capacitance of the device. Using these values, the total response bandwidth is calculated as

$$B = \frac{1}{2\pi[2 \cdot (R_C + R_S)] \cdot C}. \tag{2}$$

The contact resistance of graphene emerges from the contacts between graphene and metallic electrodes. This depends on parameters such as the quality of graphene and choice of the electrode; it was experimentally shown that the values of the contact resistivity ρ_C are in the range of 100 to 1,000 Ω μm.[29–31] The contact resistivity is expressed in a unit of Ω μm instead of the standard Ω μm^2, as the flow of carriers from the electrode to graphene occurs mostly through the contact edge.[31] Therefore, the total contact resistance of graphene is calculated as

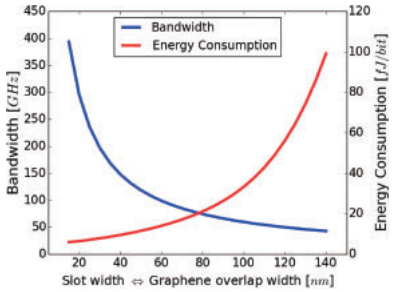

Fig. 4. Response bandwidth and energy consumption of the device with respect to different slot widths.

$$R_C = \frac{\rho_C}{L}, \tag{3}$$

where L is the length of the device [Fig. 1(a)]. In our calculations, we assumed a conservative value of $\rho_C = 1{,}000\ \Omega\,\mu\mathrm{m}$.

The graphene's sheet resistance, R_S, is usually defined through the "resistance per square" parameter, R_{SQ}. The values of R_{SQ} for graphene are typically between 100 and 500 Ω/sq;[25,32–34] in all of our calculations, we assume a conservative value of 500 Ω/sq. In order to obtain the total sheet resistance of graphene, we need to consider the parallel connection of all squares constituting the length of the device; therefore, it can be expressed as

$$R_S = R_{SQ}\frac{w_{\mathrm{El\text{–}C}}}{L} = R_{SQ}\frac{w_{\mathrm{El\text{–}WG}} + (w_{\mathrm{WG}} - w_{\mathrm{Slot}})/2}{L}. \tag{4}$$

The parameters in Eq. (4) are defined in Fig. 1(b): $w_{\mathrm{El\text{–}C}}$ is the distance between the metallic electrode and capacitor; for our device it is equal to the sum of the distance of the electrode from the edge of the waveguide ($w_{\mathrm{El\text{–}WG}}$) and length of the graphene part that covers the waveguide but is not overlapped with the opposite electrode, i.e., not switched [$(w_{\mathrm{WG}} - w_{\mathrm{Slot}})/2$]; L is the propagation length of the device, defined as in Eq. (3). In all of our calculations, we assume that the distance between the electrode and waveguide is $w_{\mathrm{El\text{–}WG}} = 1\ \mu\mathrm{m}$, which is sufficient for the metal not to disturb the optical mode. The width of the waveguide is set to $w_{\mathrm{WG}} = 540$ nm, as stated previously, while the slot width is varied as in Fig. 3.

We define the capacitance of our device as

$$C = \varepsilon_0 \varepsilon_{Al_2O_3}\frac{w_{\mathrm{Slot}} \cdot L}{d_{Al_2O_3}}, \tag{5}$$

where the employed parameters have values presented at the beginning of this paper. Equation (5) directly reveals the benefit of our design, i.e., the capacitance is proportional only to the slot width (graphene overlap), making it significantly smaller than those of previous reports, which assumed full waveguide–graphene overlap ($w_{\mathrm{Slot}} \approx 50$ nm and $w_{\mathrm{WG}} \approx 540$ nm). In our design, there is also a parasitic increase in the sheet resistance owing to the reduction of the capacitor width [Eq. (4)]. However, this increase is only approximately 10% of the resistance of previously reported devices, significantly smaller than the reduction in the capacitance. In addition, Eqs. (2)–(5) reveal that when the capacitance and resistances are multiplied, the length of the device L is canceled out; therefore, the length of the device has no impact on the response bandwidth and influences only the IL. Using the defined parameters, the bandwidth result is shown in Fig. 4. Our approach for the calculation of the response of

the device is similar to that reported by Sorianello et al. for the characterization of a graphene phase modulator design.[25)]

In addition, we calculate the average energy consumption of our device, expressed as energy per bit value; it is in the range of 5 fJ/bit for smaller slot widths, to smaller than 100 fJ/bit for larger slot widths (Fig. 4). The formula for energy per bit is:

$$E_b = \frac{1}{4} C V_b^2, \tag{6}$$

where C is the total device capacitance and V_b is the voltage required to switch the device. To calculate C from Eq. (5), we choose a device length providing 3 dB MD, considering the result in Fig. 3. Further, we choose a switching voltage required to push the Fermi level of graphene to half of the input photon energy, previously shown to be $V_b = 2.74$ V.

Figures 3 and 4 reveal the final performance of the proposed modulator with a 50 nm slot; the response bandwidth is $B = 120$ GHz, the energy per bit is $E_b = 12$ fJ/bit, the 3 dB length is $L_{3dB} = 15$ μm, and the total IL is IL = 1.4 dB. To the best of our knowledge, these are, by far, the best performance metrics of an in-line graphene modulator, demonstrating that graphene modulators have the potential to solve some of the power consumption and bandwidth issues of silicon photonics.

For completeness, we also consider the effect of the quantum capacitance of graphene, arising from its low density of states, on our modulator.[35,36)] It is a series capacitance, hence it contributes to a reduction in total capacitance and increase in speed. We neglected this capacitance in the calculation of the values plotted in Figs. 4 and 5 as it is generally not considered in characterization of graphene modulators;[13–15,25,28)] however, as it is a realistic effect, we briefly discuss its influence in this paragraph. The quantum capacitance is expressed through the formula:[35)]

$$C_Q = \frac{2e^2 k_B T}{\pi(\hbar v_F)^2} \ln\left[2\left(1 + \cosh\frac{E_F}{k_B T}\right)\right], \tag{7}$$

which reveals the quantum capacitance per electrode area. We follow the steps used for the geometric capacitance to reveal the equivalent series capacitance, yielding a bandwidth of $B = 235$ GHz for a 50 nm slot modulator, while the energy consumption is $E_b = 6$ fJ/bit. This is obtained using a small-voltage approximation; for higher voltages (higher Fermi levels), the quantum capacitance is significantly larger than the geometric capacitance and can be completely neglected. It can be shown that the inclusion of the quantum capacitance improves the performance by approximately a factor of 2 for any slot width; however, we neglect it in all of our calculations to maintain the approach of conservative assumptions.

In order to fully understand the potential of the proposed device, we also loosen the constraint of contact resistance to allow more optimistic, but still reported values.[25)] The result for the bandwidth is shown in Fig. 5; for small resistivity and slot width, the speed of the device is close to the 1 THz mark. This speed is not necessary for any commercial application; however, it demonstrates the full potential of the device and graphene modulation in general.

Fabrication challenges: Small slots can be fabricated using e-beam lithography, which is a challenge, however, they have been previously reported,[37)] and at this time, we are able to fabricate sub-100-nm slots in-house. In Fig. 1, we assume a planar surface of the waveguide, which can be obtained by depositing silicon oxide using standard plasma-enhanced chemical vapor deposition (PECVD) techniques and then performing chemical–mechanical polishing.[15)] In Fig. 1, we also assume an air slot. This enhances the slot effect, and is also more feasible in terms of fabrication as the PECVD deposition of oxide is not perfectly conformal and could not fill the slot. The graphene electrodes can be patterned using e-beam lithography and oxygen plasma, while electrodes can be fabricated in the standard lift-off process; the aluminum oxide region can be grown with atomic layer deposition (ALD). There are two main challenges to our design: 1) setting the lower graphene electrode to cover only the slot region and 2) alignment of both graphene electrodes over a sub-100-nm region of the slot. Concerning issue one, the lower graphene electrode will realistically have to cover a slightly wider region than the slot. However, it would not have to be a significantly wider region owing to the graphene's robustness,[38)] and as there is no significant change in performance if the capacitor width is increased from, for example, 50 to 70 nm, the assumption of only a slot coverage in simulations is justified. The bigger issue is the sub-100-nm alignment. In order to achieve this precise e-beam lithography, advanced resist development and etching recipes have to be developed, as well as machines with a low precision tolerance have to be used.

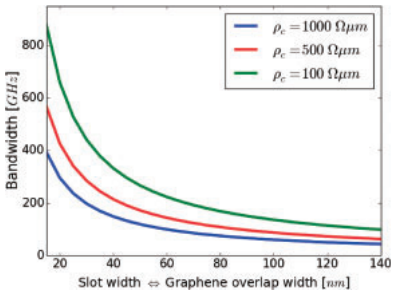

Fig. 5. Response bandwidth for different values of the contact resistivity.

In conclusion, we demonstrated an in-line graphene modulator on silicon, which could achieve response bandwidths larger than 100 GHz, with a power consumption of the order of 10 fJ/bit. We achieved this design by tailoring the overlap of the graphene electrodes, thus significantly reducing the capacitance, and consequently the RC constant of the device. In contrast to the previous methods, our method did not depend on the reduction of the graphene's resistance as we assumed conservative values for it in our calculations. The reduction of the overlap of the graphene electrodes led to an increase in the IL; however, this problem was overcome using the silicon slot waveguide. In addition, we discussed the fabrication feasibility of the proposed device; its fabrication is a large part of our future research plan. Our results show that graphene satisfies all of the requirements for large-scale implementation in silicon photonics and optical interconnects, and could pave the way for highly power- and performance-efficient short-range optical communications.

Acknowledgments The authors would like to acknowledge the financial support of the Japanese Society for the Promotion of Science through the JSPS KAKENHI Grant number 16H00902, as well as DC2 Grant-in-Aid for JSPS Fellows number 201709162 and Global Leader Program for Social Design and Management (GSDM) of the University of Tokyo.

1) K. S. Novoselov, A. K. Geim, S. V. Morozov, D. Jiang, Y. Zhang, S. V. Dubonos, I. V. Grigorieva, and A. A. Firsov, Science **306**, 666 (2004).
2) A. K. Geim and K. S. Novoselov, Nat. Mater. **6**, 183 (2007).
3) S. Sato, Jpn. J. Appl. Phys. **54**, 040102 (2015).
4) R. R. Nair, P. Blake, A. N. Grigorenko, K. S. Novoselov, T. J. Booth, T. Stauber, N. M. R. Peres, and A. K. Geim, Science **320**, 1308 (2008).
5) K. Kim, J.-Y. Choi, T. Kim, S.-H. Cho, and H.-J. Chung, Nature **479**, 338 (2011).
6) G. T. Reed, G. Mashanovich, F. Y. Gardes, and D. J. Thomson, Nat. Photonics **4**, 518 (2010).
7) X. Gan, R.-J. Shiue, Y. Gao, I. Meric, T. F. Heinz, K. Shepard, J. Hone, S. Assefa, and D. Englund, Nat. Photonics **7**, 883 (2013).
8) W. Zou, Y. Xia, W. Peng, and Y. Zeng, Appl. Phys. Express **9**, 024301 (2016).
9) Q. Bao, H. Zhang, B. Wang, Z. Ni, C. Haley, Y. X. Lim, Y. Wang, D. Y. Tang, and K. P. Loh, Nat. Photonics **5**, 411 (2011).
10) Y. Meng, S. Ye, Y. Shen, Q. Xiao, X. Fu, R. Lu, Y. Li, and M. Gong, IEEE Photonics J. **10**, 6600217 (2018).
11) X. Hu and J. Wang, IEEE J. Quantum Electron. **53**, 7200308 (2017).
12) J. Ho, S. Iwamoto, and Y. Arakawa, Jpn. J. Appl. Phys. **53**, 08MG01 (2014).
13) M. Liu, X. Yin, E. Ulin-Avila, B. Geng, T. Zentgraf, L. Ju, F. Wang, and X. Zhang, Nature **474**, 64 (2011).
14) M. Liu, X. Yin, and X. Zhang, Nano Lett. **12**, 1482 (2012).
15) C. T. Phare, Y.-H. D. Lee, J. Cardenas, and M. Lipson, Nat. Photonics **9**, 511 (2015).
16) D. Thomson, A. Zilkie, J. E. Bowers, T. Komljenovic, G. T. Reed, L. Vivien, D. Marris-Morini, E. Cassan, L. Virot, J.-M. Fédéli, J.-M. Hartmann, J. H. Schmid, D.-X. Xu, F. Boeuf, P. O'Brien, G. Z. Mashanovich, and M. Nedeljkovic, J. Opt. **18**, 073003 (2016).
17) L. Wu, H. Liu, J. Li, S. Wang, S. Qu, and L. Dong, Crystals **7**, 65 (2017).
18) J. Wang, Z. Cheng, Z. Chen, X. Wan, B. Zhu, H. K. Tsang, C. Shu, and J. Xu, Nanoscale **8**, 13206 (2016).
19) A. Phatak, Z. Cheng, C. Qin, and K. Goda, Opt. Lett. **41**, 2501 (2016).
20) G. Kovacevic and S. Yamashita, IEICE Electron. Express **13**, 20160499 (2016).
21) Y. Kim, D. W. Kim, M.-H. Lee, M. H. Lee, D. E. Yoo, K. N. Kim, S. C. Jeon, and K. H. Kim, J. Opt. **18**, 095801 (2016).
22) T. Zhang, X. Ke, X. Yin, L. Chen, and X. Li, Sci. Rep. **7**, 12169 (2017).
23) G. Kovacevic and S. Yamashita, Opt. Express **24**, 3584 (2016).
24) Y.-C. Chang, C.-H. Liu, C.-H. Liu, Z. Zhong, and T. B. Norris, Appl. Phys. Lett. **104**, 261909 (2014).
25) V. Sorianello, M. Midrio, and M. Romagnoli, Opt. Express **23**, 6478 (2015).
26) M. Mittendorff, S. Li, and T. E. Murphy, ACS Photonics **4**, 316 (2017).
27) I. Datta, C. T. Phare, A. Dutt, A. Mohanty, and M. Lipson, Ext. Apstr. Optical Society and Related Societies (CLEO Conf. 2017), 2017, Stu3N.5.
28) V. Sorianello, M. Midrio, G. Contestabile, I. Asselberghs, J. Van Campenhout, C. Huyghebaert, I. Goykhman, A. K. Ott, A. C. Ferrari, and M. Romagnoli, Nat. Photonics **12**, 40 (2018).
29) W. S. Leong, H. Gong, and J. T. L. Thong, ACS Nano **8**, 994 (2014).
30) A. Venugopal, L. Colombo, and E. M. Vogel, Appl. Phys. Lett. **96**, 013512 (2010).
31) K. Nagashio, T. Nishimura, K. Kita, and A. Toriumi, Appl. Phys. Lett. **97**, 143514 (2010).
32) J.-K. Lee, C.-S. Park, and H. Kim, RSC Adv. **4**, 62453 (2014).
33) K. C. Kwon, J. Ham, S. Kim, J.-L. Lee, and S. Y. Kim, Sci. Rep. **4**, 4830 (2014).
34) R. Ishikawa, Y. Kurokawa, S. Miyajima, and M. Konagai, Appl. Phys. Express **10**, 082301 (2017).
35) S. Khorasani and A. Koottandavida, npj 2D Mater. Appl. **1**, 7 (2017).
36) S. Dröscher, P. Roulleau, F. Molitor, P. Studerus, C. Stampfer, K. Ensslin, and T. Ihn, Phys. Scr. **2012**, 014009 (2012).
37) K. Guo, L. Lin, J. B. Christensen, E. N. Christensen, X. Shi, Y. Ding, K. Rottwitt, and H. Ou, Opt. Express **25**, 32964 (2017).
38) B. D. Briggs, B. Nagabhirava, G. Rao, R. Geer, H. Gao, Y. Xu, and B. Yu, Appl. Phys. Lett. **97**, 223102 (2010).